Two-Dimensional Crystal Structures of Protein Kinase C-δ, Its Regulatory Domain, and the Enzyme Complexed with Myelin Basic Protein

Alexander S. Solodukhin,* Heather L. Caldwell,* Julianne J. Sando,* and Robert H. Kretsinger†
Departments of *Anesthesiology and †Biology, University of Virginia, Charlottesville, Virginia 22908 USA

ABSTRACT Two-dimensional crystals of protein kinase C (PKC) δ, its regulatory domain (RDδ), and the enzyme complexed with the substrate myelin basic protein have been grown on lipid monolayers composed of phosphatidylcholine: phosphatidylserine: diolein (45:50:5, molar ratio). Images have been reconstructed to 10-Å resolution. The unit cells of all three proteins have cell edges a = b and interedge angle γ = 60°. RDδ has an edge length of 33 ± 1 Å, and its reconstruction is donut shaped. The three-dimensional reconstructions from the PKCδ C1b crystal structure (Zhang et al., 1995) can be accommodated in this two-dimensional projection. Intact PKCδ has an edge length of 46 ± 1 Å in the presence or absence of a nonhydrolyzable ATP analog, AMP-PnP. Its reconstruction has a similar donut shape, which can accommodate the C1b domain, but the spacing between donuts is greater than that in RDδ; some additional structure is visible between the donuts. The complex of PKCδ and myelin basic protein, with or without AMP-PnP, has an edge length of 43 ± 1 Å and a distinct structure. These results indicate that the C1 domains of RDδ are tightly packed in the plane of the membrane in the two-dimensional crystals, that there is a single molecule of PKCδ in the unit cell, and that its interaction with myelin basic protein induces a shift in conformation and/or packing of the enzyme.

INTRODUCTION

Protein kinase C (PKC) isozymes, a family of serine/threonine protein kinases that are activated by association with cellular membranes, are implicated in numerous intracellular signaling events (Mellor and Parker, 1998; Ron and Kazanietz, 1999). There is considerable evidence for alterations of isozyme expression and/or activity in various disease states, making these enzymes important targets for drug design. To date, though, there are very few isozyme-specific inhibitors or activators, and the mechanism of activation at the membrane is not well understood.

Most PKC isozymes fall into one of three categories based on sequence similarities and responses to cofactors (Mellor and Parker, 1998; Ron and Kazanietz, 1999). All PKCs are activated by association with acidic lipids, especially phosphatidylserine (PS), in the cell membrane. The classical or cPKCs-α, -βI, -βII, and -γ, also require calcium and diacylglycerol or phorbol esters for activity. They have four regions of similarity, constant domains C1 to C4, interspersed with variable domains, V1 to V5. Proteolysis in the V3 region generates a catalytic fragment of the enzyme, PKM, whose C3 and C4 domains are homologous, respectively, to ATP and to substrate protein binding sites in other kinases including PKA (for review, see Goldsmith and Cobb, 1994). The regulatory domain, containing C1 and C2, confers membrane binding via three segments (Oancea and Meyer, 1998; Medkova and Cho, 1999). C1 contains two cysteine-rich, Zn-binding motifs, C1a and C1b (Hubbard et al., 1991; Hurley et al., 1997), which can bind phorbol esters or diacylglycerol. Immediately N-terminal to the C1 domain is a pseudosubstrate motif that resembles a PKC substrate in having several basic amino acids; however, instead of a phosphorylatable Ser or Thr, it has an Ala (House and Kemp, 1987). This pseudosubstrate occupies the active site in C4 and must be removed by proteolysis or, more typically, membrane association to permit interaction of PKC with a substrate. The basic character of this region promotes its binding to acidic lipids in the membrane as well (Mosior and McLaughlin, 1992; Oancea and Meyer, 1998). C2 is a calcium-dependent, membrane-binding domain that has homologs in some 60 other signaling and fusion protein families (Nalefski and Falke, 1996; Hurley and Grobler, 1997).

Novel or nPKCs δ, ε, η, and θ are calcium independent. Their C2 domains are near the N terminus and do not bind calcium. The C2 domain is followed by a pseudosubstrate-C1 domain, which binds diacylglycerol and phorbol esters.

Atypical or aPKCs ξ and λ/ι (mouse/human) lack the C2 domain and have an atypical C1 domain consisting of only a single Zn-binding motif, which does not bind phorbol esters. They cannot be activated by phorbol esters and are calcium independent. Both novel and atypical PKCs have PKM catalytic domains (C3 and C4) homologous to those in conventional PKCs and other kinases.

Despite considerable effort, usable three-dimensional (3-D) crystals of intact PKC have not been obtained. The growth of microcrystals of PKCβ_1 reported by Newman et al. (1994) has not been repeated. PKC (~80 kDa) is too large for current two-dimensional (2-D) nuclear magnetic resonance analysis. However, structures are available for the C2 and C1 domains of PKCδ and for homologous catalytic (C3 and C4) domains from other proteins (Knighton et al., 1991; Hommel et al., 1994; Zhang et al., 1995;

Submitted September 12, 2001, and accepted for publication January 16, 2002.

Address reprint requests to Robert H. Kretsinger, Department of Biology, University of Virginia, McCormick Road, Charlottesville, VA 22901. Tel.: 434-982-5764; Fax: 434-982-0019; E-mail: rhk5i@virginia.edu.

0006-3495/02/05/2700/09 $2.00

Shao et al., 1996). The crystal coordinates of cAMP-dependent protein kinase (Knighton et al., 1991) have been used to model the catalytic domains of PKC (Orr and Newton, 1994).

Structures of the various domains or their homologs were used to model intact PKCα in its closed, or inactive, conformation (Srinivasan et al., 1996). However, these domain structures do not reveal structural changes upon activation of PKC at the membrane or provide direct information on the interaction between domains. They also do not address the possibility of lipid-dependent enzyme dimerization (Sando et al., 1998; Huang et al., 1999).

Recently we obtained several 2-D crystal forms of each of three PKC isozymes on lipid monolayers (Owens et al., 1998) and observed an optimum in crystal formation as a function of lipid composition (Sando et al., 1998). Here we provide a more rigorous analysis of 2-D crystals of PKCδ, of the regulatory domain of PKCδ (RDδ), and of PKCδ complexed with myelin basic protein (MBP). Reconstructed 2-D images to 10-Å resolution reveal the outline of RDδ, show that there is a single molecule of PKCδ in the unit cell, and indicate that its interaction with MBP induces a shift in conformation and/or packing of the enzyme.

MATERIALS AND METHODS

Materials

Dioleoylphosphatidylcholine (DOPC), dioleoylphosphatidylserine (DOPS), and diolein (DO) were purchased from Avanti Polar Lipids (Alabaster, AL) and were of the highest purity. MBP, lysine-rich histone, and 5′adenylylimidodiphosphate (AMP-PnP) were from Sigma (St. Louis, MO). A polyclonal antibody directed against the catalytic domain of PKCδ was obtained from Santa Cruz Biotechnology (Santa Cruz, CA). ^{3}H-Phorbol 12,13-dibutyrate (PDB), 18.6 Ci/mmol, was from NEN Life Science Products (Boston, MA). End-labeled ^{32}P-ATP was from ICN (Irvine, CA).

Purification and assay of PKCδ

PKC was purified from baculovirus-infected Sf9 insect cells by sequential chromatography on Q-sepharose and phenyl-superose as described previously (Sando and Chertihin, 1996). Baculovirus PKC constructs were generously provided by Drs. Parker, Stabel, and Fabbro. PKCδ activity was measured by transfer of phosphate from ^{32}P-ATP to lysine-rich histone or to MBP as described previously (Sando et al., 1998).

The concentration of PKC was determined by binding of PDB (Sando and Young, 1983). Yields of pure PKC varied from 2.0 to 25 nmol of protein per liter of Sf9 culture. Purity was determined by electrophoresis through 10% polyacrylamide gels after both silver staining and Western blotting using a polyclonal antibody (Santa Cruz Biotechnology) directed at a peptide in the carboxy terminus unique to PKCδ. PKC was stored in 30% glycerol at −70°C. Aliquots were thawed, diluted, and added directly to crystallization wells.

2-D crystallization

2-D crystals of RDδ, PKCδ, and PKCδ complexed with MBP and/or AMP-PnP were grown on lipid monolayers by a modification of the method of Kornberg and Darst (1991). Hemispherical wells of 30-μL volume (6-mm diameter and 2.5-mm depth) were made in a teflon block. PKCδ (48 nM) or RDδ (5.4 nM) was pipetted to the bottom of the wells with or without MBP and/or AMP-PnP (24–64 nM). 3-(*N*-morpholino)-propanesulfonic acid salt, 20 mM, pH 7.2, was added to bring the total volume to 29 μL. One microliter of freshly mixed DOPC:DOPS:DO in molar ratio of 45:50:5 (2.0 mg/mL in chloroform and hexane, volume ratio of 1:1) was gently layered over the 29 μL in the well. Wells were incubated for 3 h in darkness at 4°C.

Specimen preparation

Copper grids (300 mesh, Electron Microscopy Sciences) coated with carbon films were floated on the surface of the crystallization well for 30 s. Excess liquid was withdrawn by blotting the bottom of the grid to a filter paper. All samples were negatively stained with one drop of 1.0% w/v uranyl acetate on the dried grid for 30 s after blotting and rinsing with a drop of distilled water. Grids were dried for 1 h at ambient temperature.

Electron microscopy and image analysis

The grids were surveyed using a JEOL JEM 100CX electron microscope. Electron micrographs were taken at accelerating voltage of 100 keV at a nominal magnification of 50,000×. Electron micrographs were evaluated initially with an optical diffractometer for resolution and image quality. Selected micrographs were digitized with a film scanner (Minolta, Dimâge Scan Multi, Ramsey, NJ) at an optical resolution of 1128 dpi (22.5 μm, 4.5 Å/pixel).

We have tested several of the many software packages for 2-D crystal evaluations (Carragher and Smith, 1996; Heyman, 2001) and chosen those most suitable for each step of data processing. Fig. 1 summarizes the protocol that we have optimized.

Selection of raw field images was based on an estimation of the quality of the Fourier power spectra. The unbending and contrast transfer function determinations (Ericson and Klug, 1970) of crystalline areas were performed with the Integrated Crystallographic Environment graphical interface (Hardt et al., 1996), developed on the base of the MRC-IMAGE package (Crowther et al., 1996). Preliminary analyses of excised sections (1024 × 1024 pixels) from digitized images were made with EMTOOL software (Ludtke, 1997). Subfields of 256 × 256 pixels were padded into a 512 × 512 square field for Fourier transformation to prepare a reference image with the use of the quasioptical Fourier filtration (Klug and DeRosier, 1966) in the Micrograph Data Processing Program (MDPP) (Smith and Gottesman, 1996). An interactive procedure was used to select reflections associated with the reciprocal lattice of a single crystal in the computed diffraction pattern. This lattice was refined and used to construct a mask that passed only those Fourier coefficients that fell on reciprocal lattice points. Inverse transformation of the masked transform yielded an averaged projection of the single crystal.

Further analyses were carried out with procedures written for the SPIDER (System for Processing Image Data from Electron microscopy and Related fields) software package (Frank et al., 1996) and modified for our applications. A small area containing a centered repeating unit surrounded by one-half unit cell or more in each direction was selected from the Fourier-filtered crystalline array. This image was used as a reference for the analysis of its cross-correlation with an entire field of unprocessed images. The size of the reference image was 64 × 64 pixels. To avoid artifacts in cross-correlation functions from wrap-around overlaps implicit in the Fourier computation, the raw field and reference images were both padded into squares of 2048 × 2048 pixels. The resulting cross-correlation function contained maxima at locations in the raw image where there was a strong match with the reference. A peak search program was applied to the cross-correlation function to determine the precise coordinates of the centers of the maxima (Saxton and Baumeister, 1982), which in turn were stored in a data file in order of peak heights. A map of these peak positions

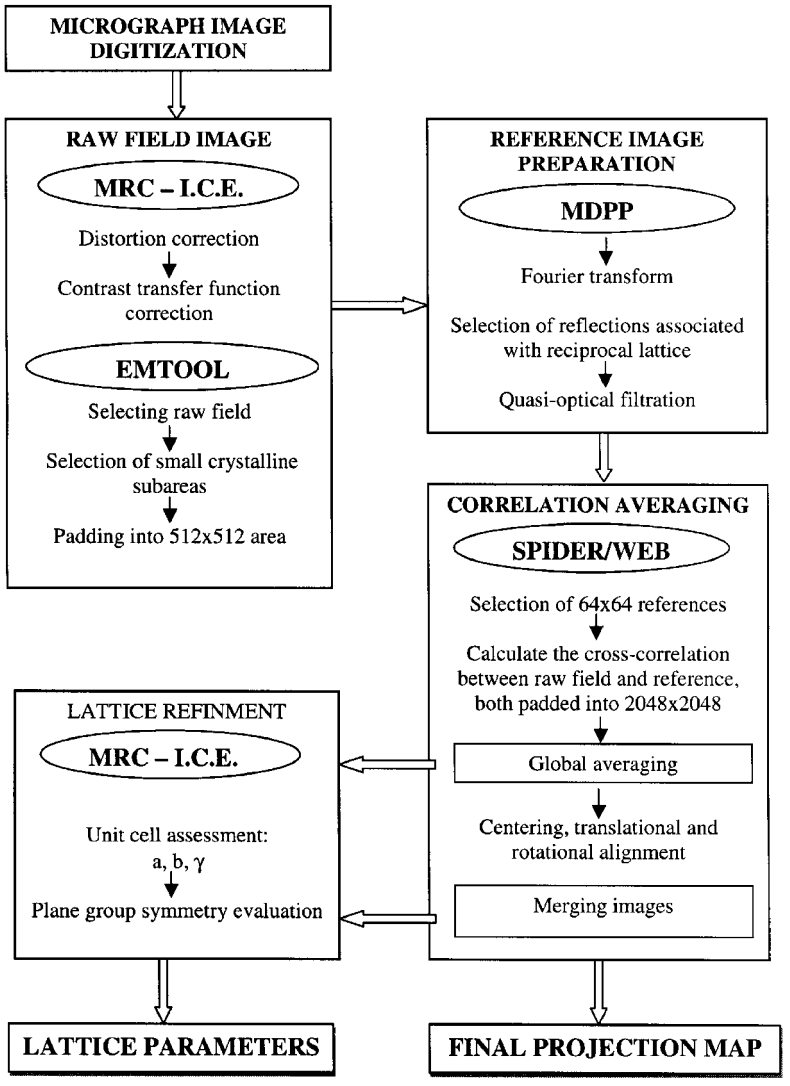

FIGURE 1 Flow diagram of the image processing procedure. The ellipses contain the titles of software packages used at each step.

was computed and displayed with a WEB program, which serves as a visualization program for the SPIDER software package. All weak points were identified by eye and removed from the peak coordinate file by an interactive procedure. Peaks with normalized correlation coefficients less than 0.7 were not processed further. The final correlation average was formed by addition of 64 × 64 pixels or larger areas extracted from the raw image at the exact positions specified by the revised peak coordinate file.

To combine projections from different crystalline areas, two correlation averages, obtained by global averaging as described above, were aligned by the following procedure. One of the two images was selected as a reference. Next, each correlation average was centered on the dyad axis at the middle of the area. This dyad was determined precisely by cross-correlating the average with itself after 180° rotation. The averages were rotationally aligned using auto correlation functions. The aligned image was checked for cross-correlation with the reference image. If differential phase residuals were less than 25°, the two images were averaged in reciprocal space; this new back transformed image was used as a reference for the next alignment cycle.

Merged images were used for the final evaluation of lattice parameters and symmetry assessment by application of SPECTRA a routine in Integrated Crystallographic Environment (Schmidt et al., 1993) and by MRC (Crowther et al., 1996), respectively. The *em2em* program (van Heel et al., 1996) was used for transporting images from one software package to another.

Overlay of the 2-D projections with 3-D surface projections from 3-D crystal studies

The Swiss-PDB Viewer 3.51 program by Glaxo Wellcome Experimental Research (www.expasy.ch/spdbv) was used for visualization of 3-D molecular structures from the Protein Data Bank and for alignment of their projections to fit with the 2-D crystal projections.

RESULTS

Analysis of PKC on the grids

Western blots of the PKCδ put into the crystallization well confirmed the absence of contamination with catalytic fragment. As shown previously, extraction of the enzyme from

the monolayer after it was lifted with the grid showed very little PKCδ (Owens et al., 1998). Over-exposure of the films during the enhanced chemiluminescence detection revealed intact enzyme on the grid; but no more than 10% of the enzyme in the well bound to the grid. At 48 nM PKCδ, the well contained 1.4 pmol, and the grid contained no more than 0.14 pmol. Similar blots also showed the presence of PKCδ on the monolayer in the presence of excess MBP substrate. We could not confirm the presence of RDδ on the grids by Western blotting because we did not have an antibody reactive with the N-terminal C1 and C2 domains. We did confirm the absence of intact PKCδ or catalytic domains in RDδ preparations by Western blotting with the C-terminal antibody, and we verified the presence and concentration of RDδ by phorbol ester binding as described in Materials and Methods (data not shown).

2-D crystals projection images and lattice parameters

In our earlier work (Owens et al., 1998) we observed three crystal lattices with each PKC isozyme examined. Here we undertook more rigorous analyses of the dominant lattice formed under optimal lipid composition (DOPC:DOPS:DO = 45:50:5; Sando et al., 1998). A portion of a raw field of PKCδ, a magnified fragment from this raw field, a typical power spectrum of the entire raw field area, and a quasioptically Fourier filtered reference image are shown in Fig. 2, *A* through *D*, respectively. A fragment of the map of a cross-correlation between the reference image and the raw field is shown in Fig. 2 *E*.

Fig. 3 shows a computer generated plot of Fourier components of the processed image of PKCδ. The amplitude of each reflection is characterized by an index of quality (IQ). IQ = 1 indicates that the signal to noise ratio is better than 7; IQ = 4 means that the ratio is between 2.3 and 1.75 (Henderson et al., 1986). The IQs of weaker reflections are indicated by a symbol not an IQ number. The resolution was determined in accordance with Glaeser and Downing (1992). Lattice parameters of 2-D crystals of RDδ, PKCδ, and PKCδ-MBP were calculated with SPECTRA (Schmidt et al., 1993). For the 5,0 reflection, the resolution is 10 Å (Fig. 3).

The unit cells of PKCδ, RDδ, and PKCδ-MBP have cell edges a ≈ b and angle γ ≈ 60° (Table 1). This suggests P3 symmetry. The results of programs (e.g., MRC-ALLSPACE) (Valpuesta et al., 1994) designed to discriminate between P1 and higher order plane groups provided phase residuals for P3 of 25° to 40° and showed a clear minimum in comparison with other groups. However, because these values generally exceed 30°, they do not strongly indicate P3. Density maps (Fig. 4, *A–C*) do not indicate threefold rotational symmetry nor are the areas of the cells large enough to accommodate three molecules. Levy et al. (1999) reported very similar angles and equal cell edges for 2-D crystals when the unit cell contains one molecule.

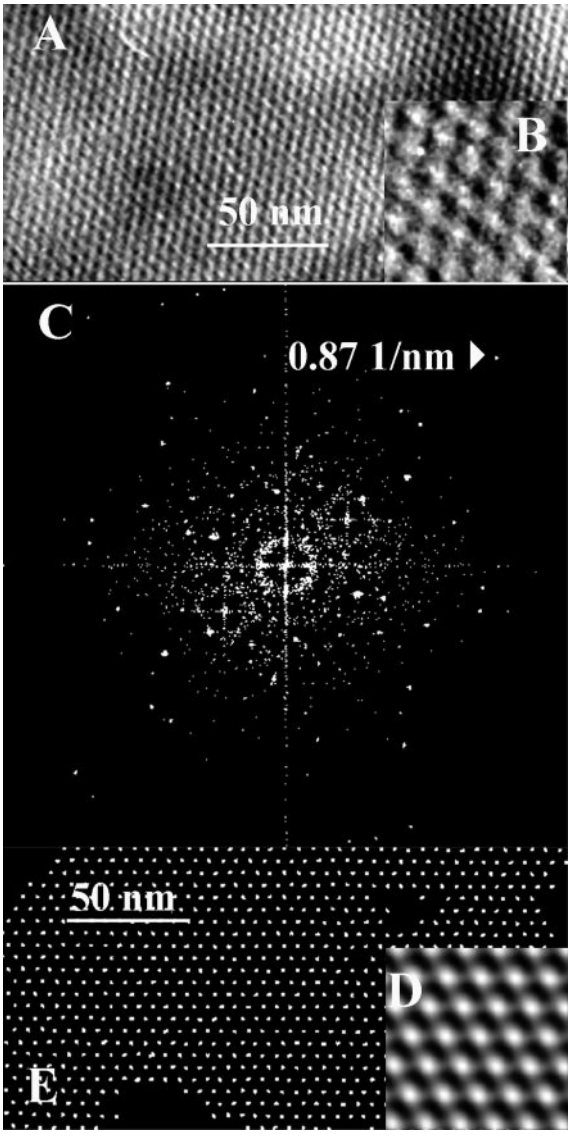

FIGURE 2 Processing of micrographs of PKCδ: (*A*) Fragment of raw field; (*B*) magnified portion of raw field; (*C*) power spectrum of Fourier transform; (*D*) reference image: the edge size is 28 × 28 nm; (*E*) fragment of the map of the cross-correlation function.

Unprocessed micrographs of crystalline areas formed by all of the investigated compounds (i.e., PKCδ, PKCδ-MBP, and RDδ) seem very similar to one another on visual inspection; however, when averaged over hundreds of unit cells, reconstructed images show striking differences in their projection maps (Fig. 4, *A–C*). The regulatory domain of PKCδ (RDδ) was subjected to similar analysis and has a smaller unit cell size (33 vs. 46 Å per side). It shows a donut-shaped structure (Fig. 4 *A*) very similar to that visualized in the images of intact PKCδ (Fig. 4 *B*); but these donuts are closely packed, whereas in intact PKCδ, they are

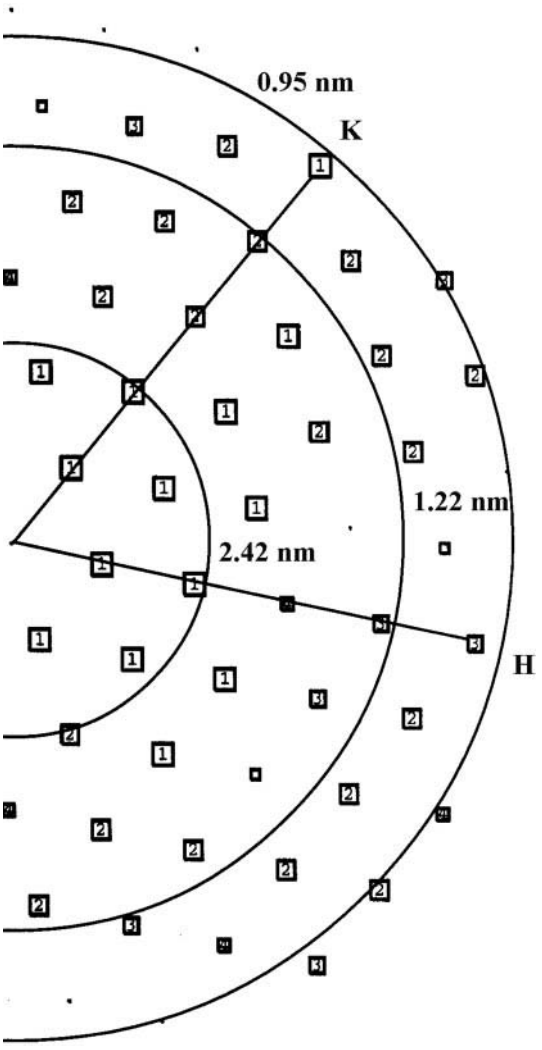

FIGURE 3 Plot of intensities of the Fourier components of PKCδ after averaging. The box sizes of individual reflections indicate their IQ values. IQ = 1 has the largest box, IQ = 8, the smallest. For clarity IQ values > 3 are not written. The circles depict the different resolution levels. Similar resolutions, not shown, were obtained for RDδ and for PKCδ-MBP.

more widely spaced and some additional structures are visible between them.

We hypothesize that the donuts represent the regulatory domain and the additional structures are contributed by the catalytic domain. To test whether this hypothesis is reasonable, we attempted to overlay the projection maps of RDδ and PKCδ with 3-D projections from the crystal structures for the PKCδ C1b (Cys2) (Zhang et al., 1995) and C2 (Pappa et al., 1998) domains. Coordinates were obtained from the Protein Data Bank (www.rcsb.org/pdb/) and fitting was performed by rotation, orientation, and tilting of the 3-D models. The C2 domain structure is too large to be accommodated in the 2-D projection of RDδ; however, the C1b domain, oriented with the phorbol ester binding site to the membrane, could be accommodated nicely in the RDδ 2-D image (Fig. 5, *A*, *C*, and *E*). The C1b domain similarly fits onto the donut structure within the intact PKCδ image but with a slightly different tilt with respect to that in RDδ (Fig. 5, *B*, *D*, and *F*).

TABLE 1 Averaged lattice parameters and cell areas

Complex	a (Å)	b (Å)	γ (deg.)	Area (Å^2)
RDδ	33 ± 1	33 ± 1	59.4 ± 0.5	940
PKCδ	46 ± 1	46 ± 1	59.8 ± 0.5	1830
PKCδ-(AMP-PnP)	46 ± 1	46 ± 1	59.6 ± 0.5	1830
PKCδ-MBP	43 ± 1	43 ± 1	59.5 ± 0.5	1600
PKCδ-MBP-(AMP-PnP)	43 ± 1	43 ± 1	60.1 ± 0.4	1600

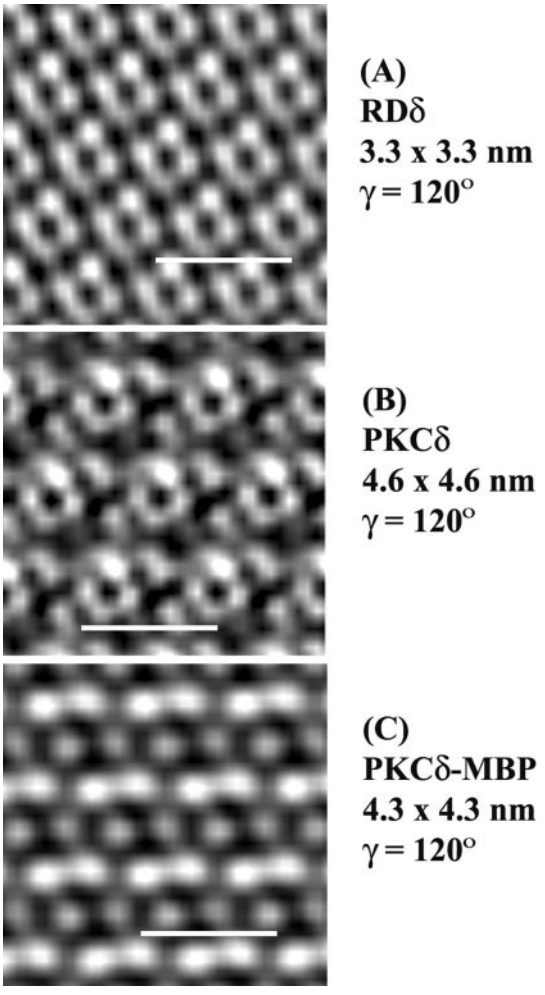

FIGURE 4 Reconstructed images of 2-D crystals: (*A*) RDδ; (*B*) PKCδ; (*C*) PKCδ-MBP. The scale bars are 5 nm.

Addition of the nonhydrolyzable ATP analog, AMP-PnP does not alter the unit cell dimensions or the appearance. Addition of a substrate protein, MBP, to PKCδ before overlaying of the lipid monolayer yields 2-D crystals whose refined image appears distinct from that of PKCδ alone (Fig. 4 *C*). No crystals of MBP without PKCδ were observed in surveys of several grids. Because the PKCδ-MBP

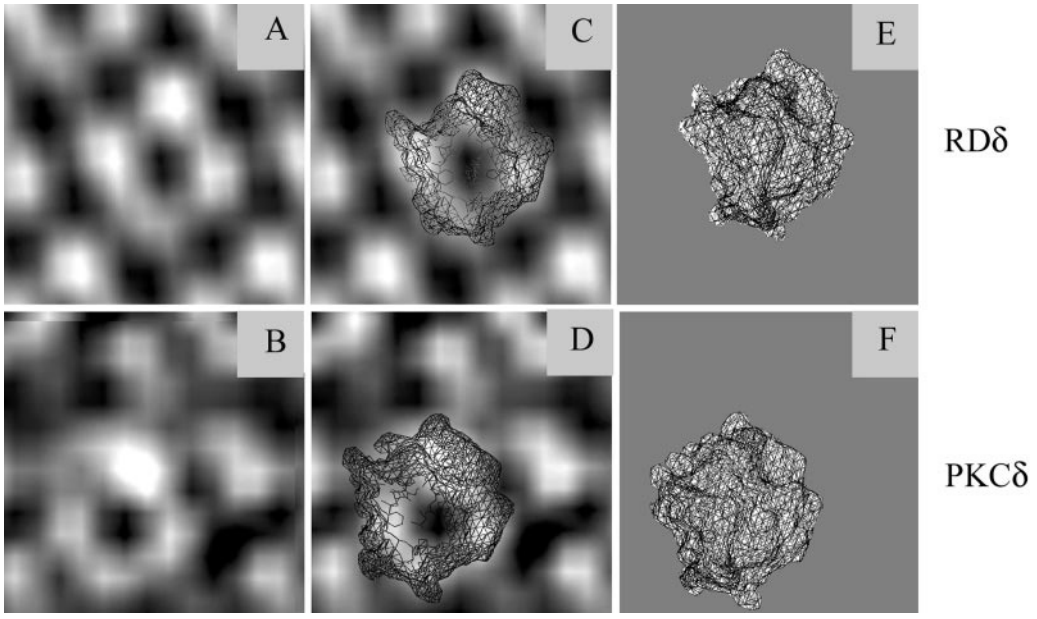

FIGURE 5 Comparison of the density maps with projections of the 3-D surface of the C1b domain of PKCδ. 2-D crystal structure reconstructions of RDδ (*A*) and of PKCδ (*B*) from electron micrographs of Fig. 4, *A* and *B*. Projections of a 10-Å cross-section slab of the 3-D crystal structure of the C1b domain superimposed on the RDδ (*C*) and on the PKCδ (*D*) reconstructions. The projections of the entire molecular surface calculated for the C1b domain and fitted to RDδ (*E*) and PKCδ (*F*) 2-D reconstructions. Fitting was performed by rotation, orientation, and slight tilting of 3-D models with the phorbol ester site oriented away from the observer. The tilt of the molecule is slightly different for PKCδ relative to RDδ. The 3-D reconstruction of C1b is based on coordinates from the NIST Protein Data Bank. These projections were computed with the Swiss-PDB Viewer software (www.expasy.ch/spdbv).

crystals have unit cell dimensions very similar to those of intact PKCδ (43 Å per side vs. 46 Å) a quantitative analysis of the differences in the images based on Fourier ring correlation and differences phase residuals calculations (Frank, 1996) was undertaken. The results of this analysis of similarity and differences of reconstructed 2-D crystalline structures of PKCδ and MBP themselves and of PKCδ versus the PKCδ-MBP complex are shown in Fig. 6, *A* through *C* and will be discussed in the next section.

DISCUSSION

In previous work, we observed three 2-D crystal forms of PKCα and δ on lipid mixtures composed of DOPC: DOPS:DO (Owens et al., 1998). An optimum in the number of PKCδ crystals per grid occurs at a lipid molar ratio of 45:50:5 (Sando et al., 1998). Using these lipid compositions, we have carried out a more rigorous analysis of the unit cell size and shape of PKCδ crystals. The PKCδ crystal of 46 ± 1 Å (Fig. 4 *B*) corresponds to the dominant 50 Å crystals we observed previously. We did not see the previously noted large crystal forms. It is possible that they represent rare enzyme multimers that do not form optimally under the standard lipid conditions. The 46-Å crystal can accommodate only monomers of PKCδ.

Rigorous analysis of large numbers of crystals allowed us to compare PKCδ with RDδ and PKCδ with substrates. The differences in unit cell dimensions and projection densities among 2-D crystals of RDδ, PKCδ, and PKCδ-MBP lend insights into domain interactions and changes in conformation that accompany binding of substrate. The significance of the inferences about molecular packing depends on a critical assessment of the resolution of the reconstructions and of the distinction among these molecular complexes.

Assessment of resolution

The simplest definition of the resolution of the reconstructed image is provided by the highest order Fourier component (Glaeser and Downing, 1992). For the (5,0) reflection in Fig. 3 the resolution is ~10 Å. Two other methods, calculation of difference phase residuals (DPR) and Fourier rings correlation (FRC), provide more rigorous assessments of resolution.

DPR, initially used in the context of single particle averaging (Frank et al., 1981), is based on a comparison of the phases of reflections in 2-D Fourier space from two independent data sets. Frank (1996) proposed using a 45° cutoff for defining the point at which the most structural information is present in the reconstruction. Using noise simulations, Glaeser and Downing (1992) showed that even with phase residuals as high as 85°, the projection maps contain useful information about the structure. We used a cutoff value of 60° as the resolution criterion for DPR analysis (Fig. 6, *A–C*). FRC is based on correlations of both phases and amplitudes. Some groups use the point at which the

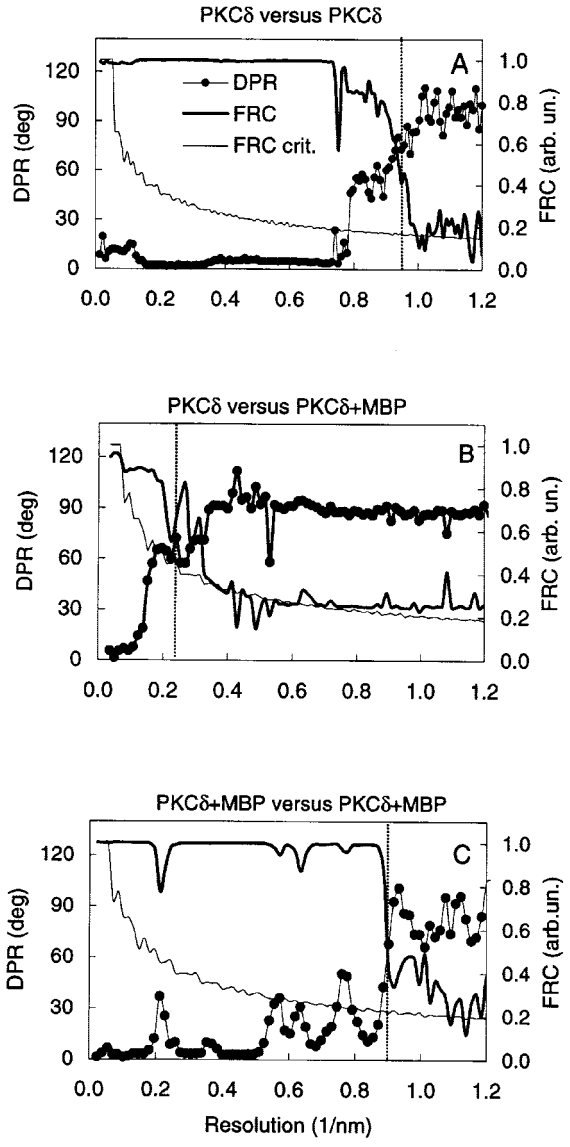

FIGURE 6 Difference phase residuals and Fourier rings correlation as a function of resolution for complexes themselves and in comparison with PKCδ: (*A*) PKCδ versus PKCδ; (*B*) PKCδ versus PKCδ- MBP; (*C*) PKCδ-MBP versus PKCδ-MBP.

correlation coefficient is 0.5 (Penczek, 1998), whereas others use the value at which the correlation curve crosses a critical FRC curve (van Heel, 1987; Orlova et al., 1997) within a standard deviation ($\pm\sigma$). The FRC critical curves of Fig. 6, *A* through *C* were calculated for pure noise with the assumption of no correlation. Penczek (1998) estimated that when the Fourier shell correlation coefficient (an analog of FRC for 3-D reconstruction) is equal to 0.5, the signal to noise ratio value becomes 1.0. We used the more conservative criterion, FRC = 0.5, rather than the 2σ one. The values of resolution estimated with DPR and with FRC are practically coincident at 10 Å (Fig. 6) and agree well with that from the highest order of Fourier component (Fig. 3).

Distinction among complexes

The cell edge lengths of PKCδ and PKCδ-MBP differ by 3 Å. To determine whether these are truly distinct we applied the DPR and the FRC techniques, described above, for quantitative analysis of similarity and differences in the species under investigation. Fig. 6 shows the DPR and the FRC for the sets of two different images as a function of spatial resolution. The phase differences between images for the same crystals are small over a wide range of spatial frequencies of Fourier components. In contrast, phase differences for Fourier components of PKCδ versus PKCδ-MBP are small only at low spatial frequencies and increase very quickly for reflections of higher than the first order (Fig. 6 *B*). This argues strongly for a significantly different packing of the enzyme in the lattice when it is bound to MBP substrate.

Comparison of PKCδ with PKCδ-(AMP-PnP) shows good phase correlation up to fourth order Fourier components, indicating a high similarity between the two images. The same result was found for PKCδ-MBP versus PKCδ-MBP-(AMP-PnP). The graphs in Fig. 6, *A* through *C* show that structural information at resolutions close to the Nyquist frequency can be obtained. Our reconstructions have resolution of $\sim$10 Å^{-1}, which is close to the value of the Nyquist frequency (Henderson, 1995).

The recovery of high-resolution information from noisy data strongly depends on the accuracy of alignment of well-defined interimage projections with respect to each other. The comparison of two subaverages originating from the same crystalline area, when no rotational alignment is needed, shows a constant FRC function and a slightly rising DPR in the region of very high resolution, indicating good phase coincidence.

Packing of PKCδ and its domains at the membrane surface

No structural information of any intact PKC is available yet for comparison with our 2-D projection images. Srinivasan et al. (1996) have modeled the structure of intact autoinhibited PKCα based on crystal structures of subdomains or their homologs from other molecules. Their model suggests a rather globular structure. A spherical PKC molecule would have a volume of $\sim 10^5$ Å^3 with a diameter of $\sim$56 Å and a circular projection image of $\sim$2460 Å^2. The area of our PKCδ unit cell is 46 × 46 Å × sin 60° = 1833 Å^2. It is too small to accommodate more than a single PKC molecule and the edge length suggests that PKC must be somewhat elongated and attached by its narrower end.

All available evidence indicates that PKCs associate with membranes via their regulatory domains (Oancea and Meyer, 1998; Medkova and Cho, 1999). The regulatory domain of PKCδ contains C2, C1a, and C1b subdomains in addition to the pseudosubstrate sequence. The dimensions

of the ellipsoid of revolution of the C2 domain, estimated with the Swiss-PDB Viewer (www.expasy.ch/spdbv) from its crystal structure (Pappa et al., 1998) are ~24 × 36 × 40 Å. Evidence suggests that calcium-binding (Nalefski and Falke, 1998) and noncalcium-binding (Garcia-Garcia et al., 2001) C2 domains interact with membranes via their larger surfaces.

The smallest cross-sectional diameter of the C1b domain of PKCδ as seen in its crystal structure (Zhang et al., 1995) from PDB files is 28 to 36 Å. This view appropriately places the phorbol ester-binding region into the plane of the membrane. These dimensions agree well with the dimensions of our RDδ 2-D projection image (~33 × 33 Å. Fig. 4). In fact, visual inspection of multiple 10-Å-thick cross-sectional slabs of the 3-D C1b domain projection reveals a remarkably good fit to the 2-D projection image (Fig. 5 *C*). The 3-D cross-section shows a donut-shaped structure very much like that of our 2-D crystals with three regions of increased density overlaying the three densest regions of our images. We assume that the C2 domain is on the other side of the C1b domain relative to the membrane. It also would seem to be distorted relative to its crystal structure and/or very tightly packed with its neighboring C2 domains.

Ochoa et al. (2001) proposed a PKC membrane-binding model in which C2 and C1b of the calcium-independent PKCs associate with the membrane with the C1a subdomain between C2 and C1b and oriented away from the membrane. This contrasts with the model for calcium-dependent PKCs, which have an opposite sequence of C1 and C2 that would place C1b between the C1a and C2 domains and oriented away from the membrane (Conesa-Zamora et al., 2000). These models are consistent with data from Medkova and Cho (1999) and Hurley et al. (1997) on phorbol ester binding of C1a or C1b in the different PKC subfamilies. C1a exhibits high affinity phorbol ester binding in calcium-dependent isozymes; whereas, C1b exhibits high affinity binding in calcium-independent PKCs. Thus, we propose that our RDδ crystals have the C1b domain associated with the membrane.

We might have expected to observe the C2 domain in contact with the membrane as well. However, Oancea and Meyer (1998) have argued that the C1 domain of PKCγ contributes the highest affinity component of the membrane binding. They argue further that this domain is immediately accessible to the membrane in the isolated regulatory domain as opposed to the intact PKC molecule. Thus, the inferred lack of contact of the C2 domain with the membrane in our 2-D crystals may be reasonable.

The 2-D images of intact PKCδ reveal a donut-shaped structure similar to that of the RDδ images. An attempt to overlay this image with a cross-section of the 3-D structure projection of the C1b domain also shows a reasonably good fit (Fig. 5 *D*). It was necessary to rotate the 3-D image slightly from that shown in the RDδ overlay to obtain the best fit. If this structure is, indeed, the C1b subdomain as we propose, the altered rotation required for optimal overlay suggests that the domain is tilted somewhat differently when packed into crystals with other components of the intact enzyme. The donuts are more widely spaced in the PKCδ images with two other regions of density interspersed. These must represent other parts of the PKCδ molecule visible in the plane of the membrane. Resolution is not yet adequate to indicate what parts of the molecule are represented by these other regions of increased density.

Inclusion of a nonhydrolyzable ATP analog does not alter significantly the size or shape of the PKCδ 2-D crystals. The quality of the currently obtained PKCδ-MBP crystals is not adequate to speculate about the orientation of any subdomains. However, it is significant that the unit cell length of intact PKCδ contracts from 46 to 43 Å and that the area decreases from 1830 to 1600 $Å^2$ upon binding of MBP, whose molecular mass is 18.5 kDa. The catalytic domain (C3 and C4, or PKM) of all PKCs is homologous to several protein kinases of known structure (Goldsmith and Cobb, 1994; Wilson et al., 1996) with principle axes of ~40 × ~46 × ~52 Å. The binding of MBP may tilt the catalytic domain so that its 52 Å axis is more nearly perpendicular to the membrane surface thereby allowing the unit cell to contract to 43 Å.

In summary, 2-D crystals of PKCδ and its regulatory domain on a lipid monolayer have provided structural information consistent with association via the C1b domain. The orientation of this domain appears similar in both RDδ and intact PKCδ with only a slight difference in the tilt. Addition of ATP does not alter significantly the structure of the membrane-bound enzyme, but addition of substrate protein decreases the unit cell size of the crystal. Future assessment of tilt series and 3-D reconstructions should further refine the structural resolution.

This work was supported by Health and Human Services grant GM31184.

REFERENCES

Carragher, B., and P. R. Smith. 1996. Advances in computational image processing for microscopy. *J. Struct. Biol.* 116:2–8.

Conesa-Zamora, J. C., J. C. Gomez-Fernandez, and S. Corbalan-Garcia. 2000. The C2 domain of protein kinase Cα is directly involved in the diacylglycerol-dependent binding of the C1 domain to the membrane. *Biochim. Biophys. Acta.* 1487:246–254.

Crowther, R. A., R. Henderson, and J. M. Smith. 1996. MRC image processing programs. *J. Struct. Biol.* 116:9–16.

Ericson, H. P., and A. Klug. 1970. The Fourier transform of an electron micrograph: effects of defocusing and aberrations, and implications for the use of underfocus contrast enhancement. *Ber. Bunsenges. Phys. Chem.* 74:1129–1137.

Frank, J. 1996. Three-Dimensional Electron Microscopy of Macromolecular Assemblies. Academic Press, San Diego.

Frank, J., M. Radermacher, P. Penczek, J. Zhu, Ya. Li, M. Ladjadj, and A. Leith. 1996. SPIDER and WEB: processing and visualization of images in 3-D electron microscopy and related fields. *J. Struct. Biol.* 116: 190–199.

Frank, J., A. Verschoor, and M. Boublik. 1981. Computer averaging of electron micrographs of 40S ribosomal subunits. *Science.* 214: 1353–1355.

Garcia-Garcia, J., J. C. Gomez-Fernandez, and S. Corbalan-Garcia. 2001. Structural characterization of the C2 domain of novel protein kinase Cϵ. *Eur. J. Biochem.* 268:1107–1117.

Glaeser, R. M., and K. N. Downing. 1992. Assessment of resolution in biological electron crystallography. *Ultramicroscopy.* 47:256–265.

Goldsmith, E. J., and M. H. Cobb. 1994. Protein kinases. *Curr. Opin. Struct. Biol.* 6:833–840.

Hardt, S., B. Wang, and M. F. Schmid. 1996. A brief description of I.C.E.: the integrated crystallographic environment. *J. Struct. Biol.* 116:68–70.

Henderson, R. 1995. The potential and limitations of neutrons, electrons and X-rays for atomic-resolution microscopy of unstained biological molecules. *Q. Rev. Biophys.* 28:171–193.

Henderson, R., J. M. Baldwin, K. Downing, J. Lepault, and F. Zemlin. 1986. Structure of purple membrane from *Halobacterium halobium*: recording, measurement and evaluation of electron micrographs at 3.5 Å resolution. *Ultramicroscopy.* 19:147–178.

Heyman, J. B. 2001. Bsoft: image and molecular processing in electron microscopy. *J. Struct. Biol.* 133:156–169.

Hommel, U., M. Zurini, and M. Luyten. 1994. Solution structure of a cysteine-rich domain of rat protein kinase C. *Nat. Struct. Biol.* 1:383–387.

House, C., and B. E. Kemp. 1987. Protein kinase C contains a pseudosubstrate prototype in its regulatory domain. *Science.* 238:1726–1728.

Huang, S.-M., P. S. Leventhal, G. J. Wiepz, and P. J. Bertics. 1999. Calcium and phosphatidylserine stimulate the self-association of conventional protein kinase C isozymes. *Biochemistry.* 38:12020–12027.

Hubbard, S. R., W. R. Bishop, P. Kirshmeier, S. J. George, S. P. Cramer, and W. A. Hendrickson. 1991. Identification and characterization of zinc binding sites in protein kinase C. *Science.* 254:1776–1779.

Hurley, J. H., and J. A. Grobler. 1997. Protein kinase C and phospholipase C: bilayer interactions and regulation. *Curr. Opin. Struct. Biol.* 7:5020–5028.

Hurley, J. H., A. C. Newton, P. J. Parker, P. M. Blumberg, and Y. Nishizuka. 1997. Taxonomy and function of C1 protein kinase C homology domains. *Protein Sci.* 6:477–480.

Klug, A., and D. J. DeRosier. 1966. Optical filtering of electron micrographs: reconstruction of one-sided images. *Nature (Lond.).* 212: 29–32.

Knighton, D. R., J. Zheng, L. F. TenEyck, V. A. Ashford, N. H. Xuong, S. S. Taylor, and J. M. Sowadski. 1991. Crystal structure of the catalytic subunit of cyclic adenosine monophosphate-dependent protein kinase. *Science.* 253:407–414.

Kornberg, R. D., and S. A. Darst. 1991. Two-dimensional crystals of proteins on lipid layers. *Curr. Opin. Struct. Biol.* 1:642–646.

Levy, D., G. Mosser, O. Lambert, G. S. Moeck, D. Bald, and J.-L. Rigaud. 1999. Two-dimensional crystallization on lipid layer: a successful approach for membrane proteins. *J. Struct. Biol.* 127:44–52.

Ludtke, S. 1997. A program for interactive image processing of electron micrographs. http://ncmi.bioch.bcm.tmc.edu/~stevel/emtool/emtool.html.

Medkova, M., and W. Cho. 1999. Interplay of C1 and C2 domains of protein kinase C-alpha in its membrane binding and activation. *J. Biol. Chem.* 274:19852–19861.

Mellor, H., and P. J. Parker. 1998. The extended protein kinse C superfamily. *Biochem. J.* 332:281–292.

Mosior, M., and S. McLaughlin. 1992. Peptides that mimic the pseudosubstrate region of protein kinase C bind to acidic lipids in membranes. *Biophys. J.* 60:149–159.

Nalefski, E. A., and J. J. Falke. 1996. The C2 domain calcium-binding motif: structural and functional diversity. *Protein Sci.* 5:2375–2390.

Nalefski, E. A., and J. J. Falke. 1998. Location of the membrane-docking face on the Ca^{2+}-activated C2 domain of cytosolic phospholipase A_2. *Biochemistry.* 37:17642–17650.

Newman, R. H., E. Carpenter, P. S. Freemont, T. Blundell, and P. J. Parker. 1994. Microcrystals of the β_1 isozyme of protein kinase C: an electron microscopic study. *Biochem. J.* 298:391–393.

Oancea, E., and T. Meyer. 1998. Protein kinase C as a molecular machine for decoding calcium and diacylglycerol signals. *Cell.* 95:307–318.

Ochoa, W. F., J. Garcia-Garcia, I. Fita, S. Corbalan-Garcia, N. Vernandez, and J. C. Gomez-Fernandez. 2001. Structure of the C2 domain from novel protein kinase C epsilon: a membrane-binding model for Ca2+-independent C2 domains. *J. Mol. Biol.* 311:837–849.

Orlova, E. V., P. Dube, J. R. Harris, E. Beckman, F. Zemlin, J. Markl, and M. van Heel. 1997. Structure of keyhole limpet hemocyanin type 1 (KLH1) at 15 Å resolution by electron cryomicroscopy and angular reconstitution. *J. Mol. Biol.* 271:417–437.

Orr, J. W., and A. C. Newton. 1994. Intrapeptide regulation of protein kinase C. *J. Biol. Chem.* 269:8383–8387.

Owens, J. M., J. J. Sando, O. I. Chertihin, and R. H. Kretsinger. 1998. Two-dimensional crystals of protein kinase C. *J. Struct. Biol.* 121: 61–67.

Pappa, H., J. Murray-Rust, L. V. Dekker, P. J. Parker, and N. Q. McDonald. 1998. Crystal structure of the C2 domain from protein kinase C-δ. *Structure.* 6:885–894.

Penczek, P. 1998. Appendix: measures of resolution using Fourier shell correlation. *J. Mol. Biol.* 280:115–116.

Ron, D., and M. G. Kazanietz. 1999. New insights into the regulation of protein kinase C and novel phorbol ester receptors. *FASEB J.* 13: 1658–1676.

Sando, J. J., and O. I. Chertihin. 1996. Activation of protein kinase C by lysophosphatidic acid: dependence on composition of phospholipid vesicles. *Biochem. J.* 317:583–588.

Sando, J. J., O. I. Chertihin, J. M. Owens, and R. H. Kretsinger. 1998. Contributions to maxima in protein kinase C activation. *J. Biol. Chem.* 273:34022–34027.

Sando, J. J., and M. C. Young. 1983. Identification of high-affinity phorbol ester receptor in cytosol of EL4 thymoma cells: requirement for calcium, magnesium, and phospholipids. *Proc. Natl. Acad. Sci. U.S.A.* 80: 2642–2646.

Saxton, W. O., and W. Baumeister. 1982. The correlation averaging of a regularly arranged bacterial cell envelope protein. *J. Microsc.* 127: 127–138.

Schmidt, M. F., R. Dargahi, and M. W. Tam. 1993. SPECTRA: a system for processing electron images of crystals. *Ultramicroscopy.* 48: 251–264.

Shao, X., B. A. Davletov, R. B. Sutton, T. C. Sudhof,. and J. Rizo. 1996. Bipartate Ca^{2+}-binding motif in C_2 domains of synaptotagmin and protein kinase C. *Science.* 273:248–251.

Smith, P. R., and S. M. Gottesman. 1996. The micrograph data processing program. *J. Struct. Biol.* 116:35–40.

Srinivasan, N., B. Bax, T. L. Blundell, and P. J. Parker. 1996. Structural aspects of the functional modules in human protein kinase-Cα deduced from comparative analysis. *Proteins Struct. Funct. Genet.* 26:17–235.

Valpuesta, J. M., J. L. Carrascosa, and R. Henderson. 1994. Analysis of electron microscope images and electron diffraction patterns of thin crystals of phi 29 connectors in ice. *J. Mol. Biol.* 240:281–287.

van Heel, M. J. 1987. Similarity measures between images. *Ultramicroscopy.* 21:95–100.

van Heel, M., G. Harauz, E. V. Orlova, R. Schmidt, and M. Schatz. 1996. A new generation of the IMAGIC image processing system. *J. Struct. Biol.* 116:17–24.

Wilson, K. P., M. J. Fitzgibbon, P. R. Caron, J. P. Griffith, W. Chen, P. G. McCaffrey, S. P. Chambers, and M. S.-S. Su. 1996. Crystal structure of p38 mitogen-activated protein kinase. *J. Biol. Chem.* 271:27696–27700.

Zhang, G., M. G. Kazanietz, P. K. Blumberg, and J. H. Hurley. 1995. Crystal structure of the Cys2 activator-binding domain of protein kinase Cδ in complex with phorbol ester. *Cell.* 81:917–924.